Magnetism of small Cr clusters: Interplay between structure, magnetic order, and electron correlations

P. Ruiz-Díaz,[1,2] J. L. Ricardo-Chávez,[3] J. Dorantes-Dávila,[1] and G. M. Pastor[2]
[1]*Instituto de Física, Universidad Autónoma de San Luis Potosí, Alvaro Obregón 64, 78000 San Luis Potosí, Mexico*
[2]*Institut für Theoretische Physik, Universität Kassel, Heinrich Plett Str. 40, 34132 Kassel, Germany*
[3]*IPICyT, Centro Nacional de Supercómputo and División de Matemáticas Aplicadas, 78216 San Luis Potosí, Mexico*
(Received 6 April 2010; revised manuscript received 9 June 2010; published 24 June 2010)

The magnetic properties of small Cr_N clusters ($N \leq 6$) are investigated in the framework of density-functional theory. The interplay between electron correlations, cluster structure, and magnetic order is quantified by performing fully spin-unrestricted calculations allowing for noncollinear spin arrangements within both the local-spin-density approximation (LSDA) and the generalized-gradient approximation (GGA). The possible transition or saddle-point states are identified by determining the vibrational frequencies from diagonalizing the dynamical matrix. In agreement with previous studies, a dimer-based growth pattern is found in all considered low-lying isomers with very short equilibrium bond lengths (typically $d_{eq}^{GGA}=1.55-1.65$ Å) alternating with relative long ones (typically $d_{eq}^{GGA}=2.75-2.85$ Å) in the relaxed geometries. Strong local magnetic moments $\vec{\mu}_i$ are, in general, obtained for the relaxed geometries (e.g., $|\mu_i^{GGA}| \simeq 2$ μ_B in Cr_4), which show a *collinear* magnetic order with antiparallel (parallel) alignment of the $\vec{\mu}_i$ along the short (long) bonds. In contrast to the GGA, the LSDA yields vanishing magnetization density in some cases ($|\mu_i^{LSDA}|=0$ $\forall$ i for $N=2$ and 4). Despite quantitative differences, both LSDA and GGA functionals always yield collinear ground-state solutions for the fully relaxed structures. In fact, noncollinear spin arrangements are found only for particular symmetric (nondimerized) geometries. However, the structures are not local minima and involve considerably large excitation energies. The results clearly indicate that the magnetic frustration, which one would physically expect in compact antiferromagnetic spin systems, is solved by *dimerization* rather than by noncollinearity of the local moments.

DOI: 10.1103/PhysRevB.81.224431 PACS number(s): 36.40.Cg, 75.75.−c, 73.22.−f, 31.15.E−

I. INTRODUCTION

Metallic magnetism and the associated electron-correlation phenomena constitute one of the major current challenges in both fundamental and applied science.[1] In past years, the study of the magnetic properties of nanostructured materials, such as clusters and nanowires, has experienced an exploiting increase in interest. This is motivated not only by the fundamental importance of low-dimensional magnetism but also by the properties of novel potential technological applications, mainly in high-density recording and storage data.[1,2] In the meantime, countless experimental and theoretical studies have demonstrated and quantified the strong dependence of magnetism on the local and chemical environment of the atoms and on the dimensionality of the systems due to electronic confinement effects. For instance, it is well known that the reduction in coordination number and the associated *d*-band narrowing yield a significant enhancement of the local spin and orbital magnetic moments as well as of the magnetic anisotropy energy.[3–7] Clusters of transition metals (TMs) with a nearly half-filled shell, such as Cr_N and Mn_N, are particularly interesting in this context since their large number of carriers per atom opens the possibility of developing huge local spin polarization.[8–10] However, the tendency to antiparallel alignments between nearest-neighbors (NN) moments, which is characteristic of half-band filling, and the tendency to form compact structures which is characteristic of strongly bonded clusters, are often the source of magnetic frustrations and instabilities which can lead to noncollinear (NC) spin arrangements or structural distortions.[11] The proper characterization of the interplay between structure and magnetism is therefore most interesting in these systems.

Electron correlation effects in half-filled band magnetic clusters have been previously investigated using many-body models.[10,12] From the point of view of *ab initio* methods, it is also important to quantify the role of electron-correlation effects by comparing different exchange-correlation (XC) functionals. In particular, chromium clusters have been the subject of remarkable experimental and theoretical research activities over the past years. Early experimental measurements[13,14] determined that the Cr dimer has a short bond length of 1.6788 Å, which is considerably smaller than that of bulk. More recently, Payne *et al.*[15] measured the magnetic moment of free-standing Cr clusters up to $N<133$ atoms showing that Cr has an unique and complex behavior as a function of cluster size, namely, the formation of two different magnetic behaviors. Understanding these remarkable findings remains nowadays a challenge. From the point of view of theory, most studies have been focused on structural and magnetic properties,[16–24] considering collinear magnetic arrangements and usually taking only into account the local-spin-density approximation (LSDA).[20,21,24] The majority of the available theoretical results on Cr_N clusters have clearly shown that the optimal structure presents a dimerlike growth.[20,23,24] For example, collinear LSDA calculations by Cheng and Wang[20] and Martínez and Alonso[24] show that Cr clusters exhibit a dimer-growth behavior until $n \leq 11$ and that a bcc bulklike growth beyond those sizes takes place.[20] By using density-functional theory (DFT) within generalized-

gradient approximation (GGA) and assuming only collinear spin arrangements, Wang *et al.*[23] found significant differences for the ground-state structures of Cr_N ($N \leq 5$) with those obtained by Cheng and Wang.[20] In addition, the dimer-like pattern was found only for $N \leq 4$. Kohl and Bertsch[25] studied Cr clusters up to 13 atoms by using pseudopotentials and by allowing noncollinear spin configurations within the LSDA. A simulated annealing technique was used for the structure optimization. They obtained that Cr clusters favor noncollinear spin arrangements. However, no dimer-growth route was found on their calculations. By using different exchange-correlation functionals and by fixing the interatomic distance for some coplanar structure (no relaxation of the atomic geometry), Peralta *et al.*[26] found noncollinear arrangements in small Cr_N ($N=3$, 5, 7, and 12).

Despite the intense research activity, there is no available study to our knowledge, in which noncollinear spin configurations, correlation effects, and structure optimization are considered on the same footing. The purpose of this work is therefore to perform an exhaustive and systematic study of the underlying interplay between the structure and magnetism in small Cr clusters having size $N \leq 6$ atoms. To this aim, a thorough exploration of the various possible collinear and noncollinear magnetic configurations is performed by taking into account geometry relaxation and the structural dependence rigorously on the same footing. The role of exchange and correlation effects on the magnetism of Cr clusters is investigated by comparing LSDA and GGA functionals. The remainder of the paper is organized as follows. In Sec. II the theoretical background is briefly recalled together with some specific details of the calculations. The main results are presented and analyzed in Sec. III considering the behavior of each cluster size in some detail. General trends in the behavior of structural and magnetic properties of small Cr clusters are discussed in Sec. IV. Here, we focus, in particular, on the role played by exchange and correlation functionals, as well as on the interplay between different magnetic orders.

II. THEORETICAL METHODS

In the following we briefly outline the theoretical background of the unrestricted spin-density functional method used for investigating the magnetic properties of small Cr clusters. Emphasis is given to the treatment of noncollinear spin arrangements and to the relative stability of collinear and noncollinear solutions of the Kohn-Sham equations. In addition some details specific to the present work are pointed out.

The calculations are performed in the framework of Hohenberg-Kohn-Sham's density-functional theory[27] as implemented in the Vienna *ab initio* simulation package (VASP).[28] This computer code solves the spin-polarized Kohn-Sham (KS) equations[27] in an augmented plane-wave basis set by using the projector augmented wave (PAW) method,[29,30] which is an approximate all-electron approach with frozen cores. For 3*d* TMs, electronic and magnetic properties are accurately described by considering 3*d*, 4*s*, and 4*p* electrons as valence states.[29,30] The exchange and the correlation effects are treated in the LSDA and the GGA (Refs. 31 and 32) by using, respectively, the Vosko-Wilk-Nussair and the Perdew-Burke-Ernzerhof functionals.[33–35] The clusters are placed inside of a simple cubic supercell whose dimensions are such that the interactions between neighboring images are negligible. In practice, this criterion is satisfied when the images are separated from each other by at least 12 Å. The KS wave functions in the interstitial region are expanded in a plane-wave basis set with a kinetic-energy cutoff of 337.3 eV. This value guarantees that, for the considered clusters, the total energy is converged within less than 1 meV/per atom. For metalliclike systems, one often finds very rapid variations in states close to the Fermi level that may cause a poor convergence of relevant physical quantities such as the total energy. Therefore, a smearing of the KS levels is introduced in order to improve numerical stability. We have used a Gaussian smearing method[36] with a very small final standard deviation $\sigma=0.005$ eV, which keeps the entropy of the noninteracting KS gas below 10^{-6} eV/K atom. The calculation of all properties is carried out by considering only the Γ point in reciprocal space since we are dealing with isolated clusters. The geometry optimization is performed by using the conjugate-gradient and quasi-Newton methods until all the forces on each atom are less than 0.005 eV/Å. Moreover, for each stationary point of the total-energy surface (i.e., for each relaxed structure having a nearly vanishing $\|\vec{\nabla}E\|$), we determine the vibrational frequencies from diagonalizing the dynamical matrix. The latter is calculated from finite differences of the analytic gradients of the total energy. In this way we can rule out saddle points (SP) (transition states) to which the local optimization procedure happens to converge on some occasions.

Local properties, such as charges and magnetic moments, are determined within the noncollinear formalism of DFT, in which the charge-density spin matrix $\rho_{\alpha\beta}(\vec{r})$ is the fundamental variable, and the Kohn-Sham orbitals are represented by spinors.[37] For instance, the charge density $n(\vec{r})$ and the magnetization density $\vec{m}(\vec{r})$ are given by

$$n(\vec{r}) = \mathrm{Tr}[\rho_{\alpha\beta}(\vec{r})] = \sum_{\alpha} \rho_{\alpha\alpha}(\vec{r}) \tag{1}$$

and

$$\vec{m}(\vec{r}) = \sum_{\alpha\beta} \rho_{\alpha\beta}(\vec{r}) \cdot \vec{\sigma}_{\alpha\beta}, \tag{2}$$

where $\vec{\sigma}=(\sigma_x,\sigma_y,\sigma_z)$ refers to the Pauli matrices. In order to search as thoroughly as possible for collinear and noncollinear solutions of the Kohn-Sham equations a large number of different spin configurations have been considered as starting points for the numerical iterations. First of all, by optimizing the structure and a systematic search of collinear solutions is performed by varying at the same time the total spin moment S_z in its full range $0<S<3N$. The resulting relaxed structures and collinear spin configurations are then used as starting points of fully unrestricted noncollinear calculations. Small random variations in the atomic positions and local moment orientations are introduced, which allow to test the stability of collinear solutions and to infer possible noncollinear arrangements in the interstitial region. In addi-

TABLE I. Equilibrium distance d_e (in Å), cohesive energy E_{coh} (in eV/atom), local magnetic moments μ_i (in μ_B, $i=1,2$), and total spin moment $2S_z$ of Cr_2. Results are given for LSDA and GGA XC potentials. The vibrational frequency ν_0 (in cm^{-1}) is also given for the GGA potential.

XC	d_e	E_{coh}	μ_1	μ_2	$2S_z$	ν_0
LSDA	1.47	3.79	0.0	0.0	0.0	
GGA	1.59	1.77	2.0	−2.0	0.0	419.71

tion, a number of truly noncollinear starting spin configurations (typically 20) are considered. This includes the magnetic order reported in previous studies,[20,21,23–25,38] random orientations of the $\vec{\mu}_i$, together with the NC spin orders obtained by varying the parameters of a self-consistent *d*-band Hamiltonian model.[39,40]

It is important to remark that in all cases, i.e., for all S_z and for all starting noncollinear configurations, the geometry has been optimized following the forces resulting from the self-consistent solution of the KS equations. This is the relevant method in order to determine the most stable structure, total spin moment S_z, and the associated magnetic order, since relaxations of geometric, electronic, and magnetic degrees of freedom need to be treated on the same footing. However, notice that the procedure precludes one from obtaining interesting complex spin arrangements which, though corresponding to the electronic ground state for a given fixed structure, would yield nonvanishing interatomic forces. An interesting example of this kind of problem has been demonstrated by Rollmann *et al.*,[41] who showed that certain noncollinear spin arrangements found in Fe_5 by Oda *et al.*,[42] are less stable than collinear spin orders once the global optimal cluster geometry is considered. Identifying possible noncollinear spin arrangements in geometries that are not optimal, would be relevant in order to explore the complex energy landscape of these clusters in view of, for example, finite-temperature simulations.

The local magnetic moments are computed by integrating the magnetization density in the PAW sphere of each atom, which for Cr has a radius of $r_{\mathrm{PAW}}=1.3$ Å. In addition, an analysis using Bader atomic cells[43] has been performed in order to check the accuracy of the values of the local magnetic moments. In all cases the Bader calculations give the same trends as the PAW method. Therefore, we focus in the following on the results obtained inside the PAW spheres.

III. RESULTS

In this section, we discuss the results obtained for Cr_N clusters ($N\leq 6$) by using LSDA and GGA approximations. For each cluster size, we analyze the results by focusing mainly on the interplay between structure and magnetic properties and electronic correlations. The case of Cr_2 is discussed with special detail, since the elementary dimer constitutes the cornerstone for understanding the nature of structural and magnetic behaviors of small Cr clusters. The structural relaxation is carried out by taking into account all the possible topologies, allowed by graph theory, as starting geometrical configurations. Finally, our results are compared with previous calculations whenever available.[20,21,23–26,44]

A. Cr dimer

The Cr dimer has been the subject of numerous investigations by using a variety of theoretical and experimental techniques. It therefore constitutes an important test for the reliability of any method of calculation.[16,18,19] Moreover, as it will be discussed below, understanding Cr_2 is crucial for the interpretation of the main results of the present work. Let us first recall that experiment shows that Cr_2 has a singlet ground state with a dominantly *d-d* chemical bond leading to very short equilibrium distance $d_e^{\mathrm{exp}}=1.67\pm0.01$ Å.[13,14,45] Although this is far below the typical bond length for most TM dimers, one does not observe a very strong bonding. The measured dissociation energy is $E_{\mathrm{coh}}^{\mathrm{exp}}=0.72$ eV/atom,[46] which is not as large as one would expect for such short distance. Actually, the binding energy for Cr_2 is smaller than for Cu_2 [$E_{\mathrm{coh}}^{\mathrm{exp}}(Cu_2)=1.039$ eV/atom (Ref. 47)] indicating that in Cr_2 the chemical bond strength is relatively weak.[18] Most of the subtle magnetic behavior of Cr_2 comes from these unusual properties. Early theoretical attempts to explain these experimental results, by means of quantum-chemical and DFT approaches, were able to describe neither the bond length nor its physical nature. This was in part due to the relatively small size of the considered basis sets[16,48] and to the very large number of many-body determinants or configurations needed to be included in the explicitly correlated quantum chemical calculations. Nowadays, however, it is well established that most DFT implementations describe the Cr_2 bonding in agreement with experiment.[18,49–51]

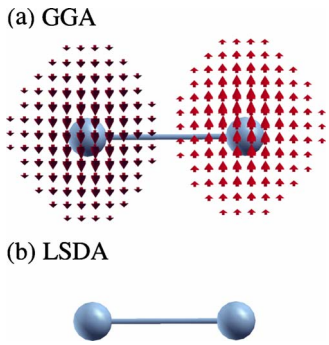

FIG. 1. (Color online) Ground-state magnetization density distribution $\vec{m}(\vec{r})$ inside the PAW spheres in Cr_2 as obtained by using (a) GGA and (b) LSDA to exchange and correlation functionals at their respective equilibrium distance.

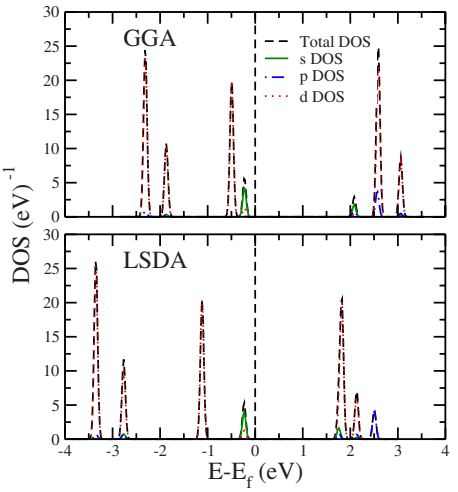

FIG. 2. (Color online) Local density of states $\rho_i(E)$ at one of the atoms of Cr_2, as well as orbital-projected density of states $\rho_i(E)$ for $\alpha=s$, p, and d. The results are obtained using (a) GGA and (b) LSDA.

Our results for Cr_2 are summarized in Table I. Using the GGA we find a short bond length $d_e^{\mathrm{GGA}}=1.59$ Å, in qualitative agreement with the experimental results and previous calculations. The corresponding cohesive energy is $E_{\mathrm{coh}}^{\mathrm{GGA}}=0.885$ eV/atom, which is close to the experimental value $E_{\mathrm{coh}}^{\mathrm{exp}}=0.72$ eV/atom.[46] The LSDA yields an even shorter bond length $d_e^{\mathrm{LSDA}}=1.47$ Å and a much larger cohesive energy $E_{\mathrm{coh}}^{\mathrm{LSDA}}=1.89$ eV/atom, which reflects the excessive overbinding often found with the local XC functional. The calculated vibrational frequency is $\nu_0=419.71$ cm^{-1} which is somewhat smaller than the experimental finding ($\nu_0^{\mathrm{exp}}=480\pm0.05$ cm^{-1}). Concerning the magnetic properties, the ground state derived in both, GGA and LSDA, has a vanishing total spin moment $S_z=0$. In the GGA this corresponds to a broken-symmetry antiferromagnetic (AF) state with large collinear antiparallel atomic moments, which value within the PAW sphere is $\mu=\pm2$ μ_B. In contrast, the LSDA shows no traces of spin polarization at all $[m(\vec{r})=0,\ \forall\ \vec{r}]$. These results are in good agreement with previous theoretical works.[20,21,24] A more detailed analysis of the GGA magnetization density in Cr_2 shows a truly collinear antiparallel alignments of the local moments, since $m(\vec{r})$ always points in the same direction, at all points $\vec{r}$ inside the PAW spheres of the two atoms [see Fig. 1(a)].

A question that often arises when comparing the outcome of different XC functionals is to discern the extent to which these differences are purely due to a different description of electronic correlations or if they are largely a consequence of the different equilibrium bond lengths, or more generally, of the cluster structure. In order to explore the matter in more detail we have also performed calculations by using the LSDA functional with the somewhat larger LSDA equilibrium distance, and vice versa. The results show indeed that the LSDA solution becomes magnetic at the GGA distance with antiparallel local magnetic moments $\mu_i=\pm1$ μ_B on each atom (AF order). In contrast, the GGA solution remains AF at the shorter LSDA equilibrium distance, although the size of the local moments decreases to $\mu_i=\pm1.5$ μ_B. This

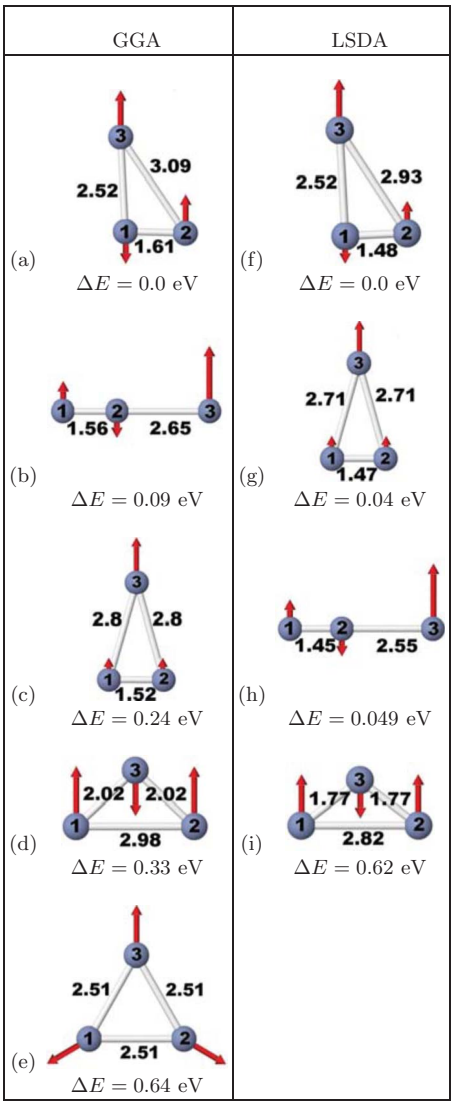

FIG. 3. (Color online) Illustration of the different isomers of Cr_3 found using the GGA and the LSDA. Results are given for the equilibrium bond lengths d_e^{ij} (in Å) and for the energy difference ΔE (in eV) with respect to the optimal structure for each XC functional. The numbers label the different atoms, which local moments are given in Table II.

illustrates the subtle interplay between hybridization and electronic correlations in Cr_2. A similar qualitative behavior was also found in bulk Cr.[52] One concludes that the local functional favors interatomic hybridizations over intraatomic exchange interactions thus stabilizing a strongly bonded nonmagnetic state with respect to a magnetic configuration with a weaker chemical bond.

In order to gain further insight on the electronic properties of Cr_2, it is interesting to consider the local ρ_i and the orbital-resolved $\rho_{i\alpha}$ Kohn-Sham densities of states. In Fig. 2 results are given for $\rho_{i\alpha}$ corresponding to the LSDA and the GGA, from which information of the dominant bonding mechanisms can be inferred. The character and degeneracy of both LSDA and GGA $\rho_{i\alpha}$ point to a sextuplet bond of mainly d and s types (sextuplet) with minor contributions from mixed sd orbitals and nearly negligible p contributions. Notice the

TABLE II. Local magnetic moments μ_i and average moments $\bar{\mu}$ (in μ_B) of the stable isomers of Cr_3 as illustrated in Fig. 3. GGA and LSDA results are compared. For the noncollinear state [Fig. 3(e)] the absolute value of μ_i is meant. The SP and the DSP are specified.

Structure	XC	μ_1	μ_2	μ_3	$\bar{\mu}$
(a)	GGA	−1.83	2.18	4.44	2.0
(f)	LSDA	−0.52	0.87	4.43	2.0
(b)	GGA	2.0	−1.74	4.52	2.0
(h)	LSDA	0.82	−0.50	4.46	2.0
(c)	GGA	0.12	0.12	4.48	2.0
(g)	LSDA (SP)	0.16	0.16	4.45	2.0
(d)	GGA (SP)	3.77	3.77	−2.70	2.0
(i)	LSDA (SP)	3.15	3.15	−1.32	2.0
(e)	GGA (DSP)	4.1	4.1	4.1	0.0

large highest occupied molecular orbital-lowest unoccupied molecular orbital gaps and the quantitative differences between LSDA and GGA results. As it will be discussed below, this close-shell-like behavior is probably at the origin of the dominant dimer-based growth and antiferromagnetic couplings found in larger clusters.

B. Trimers

In the case of Cr_3, the linear chain, as well as equilateral, isosceles (acute and obtuse), and rectangular triangles are considered as starting points of the geometry optimization. Illustrations of the most stable isomers of Cr_3 and their magnetic order are shown in Fig. 3. Here, ΔE refers to the total energy of the corresponding isomers relative to the ground-state energy. The corresponding values of the local and average magnetic moments are given in Table II.

Let us first consider the results obtained by using the GGA functional. The ground-state structure is a slightly distorted rectangle with only reflexion C_s symmetry. It is formed by a dimer with a short bond length of $d_e^{1,2}=1.61$ Å and antiparallel moments ($\mu_1=-1.83$ μ_B and $\mu_2=2.18$ μ_B) and a third atom, having a magnetic moment $\mu_3=4.44$ μ_B, at distances of $d_e^{1,3}=2.52$ Å and $d_e^{2,3}=3.09$ Å to the two atoms of the dimer. The closest isomer ($\Delta E=0.09$ eV) corresponds to the linear chain with a collinear AF-like coupling between the atomic magnetic moments. As in the optimal geometry, one finds an atom with a relatively large local moment $\mu_3 \simeq 4.52$ μ_B that is weakly coupled to a dimer ($d_e^{2,3}=2.65$ Å) in which the bond length is short ($d_e^{1,2}=1.56$ Å) and have antiparallel local moments ($\mu_1=2.0$ μ_B and $\mu_2=-1.74$ μ_B). The following isomer is an isosceles acute triangle (C_{2v} symmetry) showing a collinear FM-like arrangement and an energy difference of $\Delta E=0.24$ eV with respect to the ground state. Then follows a saddle-point (an obtuse isosceles) triangle with a collinear AF-like magnetic configuration ($\Delta E=0.33$ eV). All these collinear configurations have an average magnetic moment of $\bar{\mu}=2$ μ_B. Notice that there appears to be no simple rule between the magnetic coupling and the bond length. Sometimes the coupling is AF along short bonds [see Figs. 3(a), 3(b), and 3(d)] and sometimes the opposite trend holds [Fig. 3(c)]. It is rather the interplay between different magnetic coupling and geometries what appears to define the relative stability of the various configurations. In addition, we also have searched for noncollinear spin configurations in all the considered structures. The lowest lying isomer having noncollinear moments is an equilateral triangle with a rather

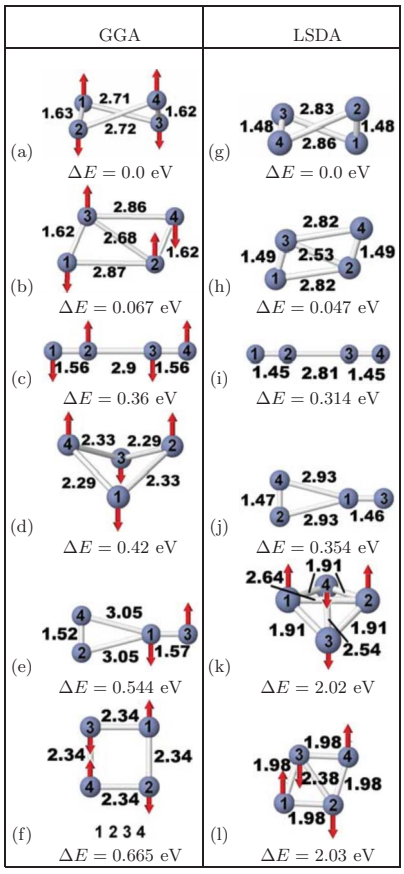

FIG. 4. (Color online) Illustration of the different isomers of Cr_4 found using the GGA and the LSDA. Results are given for the equilibrium bond lengths d_e^{ij} (in Å) and for the energy difference ΔE (in eV) with respect to the optimal structure for each XC functional. The numbers label the different atoms, which local moments are given in Table III.

TABLE III. Local magnetic moments μ_i and average moments $\bar{\mu}$ (in μ_B) of the stable isomers of Cr_4 as illustrated in Fig. 4. GGA and LSDA results are compared. The SP are specified.

Isomer	XC	μ_1	μ_2	μ_3	μ_4	$\bar{\mu}$
(a)	GGA	2.0	−2.0	−2.0	2.0	0.0
(g)	LSDA	0.0	0.0	0.0	0.0	0.0
(b)	GGA	−1.98	1.98	1.98	−1.98	0.0
(h)	LSDA	0.0	0.0	0.0	0.0	0.0
(c)	GGA	1.94	−1.8	1.8	−1.94	0.0
(i)	LSDA	0.0	0.0	0.0	0.0	0.0
(d)	GGA	−3.71	3.71	−3.71	3.71	0.0
(k)	LSDA(SP)	1.81	1.81	−1.29	−1.29	0.5
(e)	GGA (SP)	−1.81	−0.02	1.88	−0.02	0.0
(j)	LSDA (SP)	0.0	0.0	0.0	0.0	0.0
(f)	GGA (SP)	3.827	−3.827	−3.827	3.827	0.0
(l)	LSDA (SP)	2.11	−2.04	−2.04	2.11	0.0

large isomerization energy $\Delta E=0.64$ eV. This structure and the corresponding magnetic configuration has been already reported in Ref. 44. Notice the enhancement of the local magnetic moments with respect to the collinear solutions. Here, due to noncollinearity, a vanishing average magnetic moment $\bar{\mu}=0$ is obtained. However, a careful analysis of the vibrational frequencies show that this structure corresponds to a double SP (DSP).

The linear chain and the triangles (b) and (c) in Fig. 3, which show a collinear magnetic order, have a clear tendency to form dimers with a bond length that is similar to that of the isolated dimer. In these cases, the equilibrium position of the third atom lies away from the dimer, at a distance that is even larger than that of bulk Cr, where it develops a very large, almost saturated (atomiclike) magnetic moment $\mu_3 \simeq 4.5$ μ_B. The magnetic coupling between the two atoms forming the dimer or between NN atoms with short distance is, in general, AF-like with important through nonsaturated local magnetic moments [e.g., $\mu_1 \simeq 2$ μ_B in Fig. 3(a) and $\mu_1 \simeq 2$ μ_B in Fig. 3(b)]. However, in the acute isosceles triangle [Fig. 3(c)] this coupling as well as the coupling with μ_3 is FM-like. This parallel alignment of all moments is accompanied by a strong reduction in the local moments μ_1 and μ_2. Moreover, notice that bonds having parallel local moments [e.g., μ_2 and μ_3 in (a), μ_1 or μ_2 and μ_3 in (c)] are always quite large, typically $d_e=2.8-3.0$ Å, i.e., larger than the bulk Cr NN distance. In the case of the obtuse triangle, which results to be a saddle point, no dimer with a very short bond length is singled out. Instead, two symmetric bonds are formed having not too short equilibrium distance $d_e^{1,3}=d_e^{2,3}=2.0$ Å and antiparallel orientation of the local moments. Since full AF coupling is frustrated, the atoms having parallel moments μ_1 and μ_2 tend to separate from each other to a distance larger than that of bulk Cr. Noncollinear magnetic arrangements are not favored in the low-lying isomers. The tendency to form dimers with AF coupling[44] and short bond lengths dominates. It seems that the NC order involves large spin polarizations, which require a significant expansion of the interatomic distances leading to a reduced binding energy. Nevertheless, the noncollinear magnetism in Cr clusters might still be possible for more excited isomers having larger bond lengths or in the case of clusters deposited on surfaces.[53] Comparing our results with other GGA calculations, we obtain similar results as previous calculations by Wang *et al.*[23] within Gaussian. In fact, they obtain the same ground-state structure, namely, a triangle with the C_s symmetry with two atoms forming an AF dimer at a distance of 1.71 Å and the third atom lying at 2.91 and 2.39 Å to the other two atoms and with a total magnetic moment of 6 μ_B. In contrast, Kondo *et al.*[21] using Amsterdam density-functional method found a triangle with the C_{2v} symmetry as the ground-state geometry and no dimerization.

It is interesting to contrast the GGA results with the outcome of the simpler LSDA functional in order to infer the role of XC effects on magnetic and structural properties as well as the former calculations. For a given type of topology (e.g., linear chains, acute or obtuse triangles), LSDA and GGA magnetic orders are qualitatively similar. As in the case of the dimer the LSDA bond lengths are systematically shorter and the local magnetic moments are almost always smaller. Although the optimal geometry in both, the LSDA and GGA, is the nearly rectangular triangle, there are some important differences in the relative stability of the low-lying isomers.

In the LSDA the first excited stationary state is the isosceles acute triangle, which is almost degenerate with the linear chain ($\Delta E=0.009$ eV). However the analysis of the vibrational frequencies in this structure yields that this stationary state is a saddle point. Most probably this geometry corresponds to a transition state between two scalene triangles in which the edge formed by atoms 1 and 3 [see Fig. 3(f)] is opposite. The results for the optimal structure are in qualitative agreement with previous LSDA theoretical studies. Cheng and Wang[20] and Martínez and Alonso[24] obtained similar results for the ground-state structure (C_{2v} symmetry) with vanishing magnetic moments at the dimer. Martínez and Alonso[24] obtained also the dimerized isosceles triangle with an average magnetic moment $\bar{\mu}=1.5$ μ_B. It is important to remark that in our LSDA calculations we only obtained collinear arrangements, which contrasts with the re-

sults reported by Kohl and Bertsch[25] who obtained a noncollinear solution for the C_{2v} symmetry ground-state structure. Moreover, the noncollinear configurations, reported by Kohl and Bertsch[25] as ground states, have been reproduced in the present study if we assume exactly the same structure. However, in this case one obtains a much higher energy than in the relaxed structures. If these structures are relaxed, the noncollinear arrangements always disappear, giving rise to more stable structure with collinear magnetic configurations.

C. Tetramers

For Cr_4 clusters all the topological structures have been considered as starting geometries for the relaxation process. We proceed as before by discussing first the results obtained with the GGA functional. Results for the low-lying isomers and magnetic moments are reported in Fig. 4 and Table III. The most stable geometry we obtain is a twisted two-dimer structure with D_2 symmetry. In practice, if one starts with a regular tetrahedron, the configuration is unstable and as a result of relaxation, the converged solution shows two distinct dimers separated by relatively large distance. Within each dimer one finds AF-like coupling and a short bond length similar to that of Cr_2. In this isomer the local magnetic moments are collinear and compensate each other, so that the total magnetic moment vanishes. It should also noted that the binding energy between short distances in Cr_4 is much weaker than in Cr_2 despite the fact the number of bonds is four [$\Delta E_B = 2E(Cr_2) - E(Cr_4) = 0.94$ eV in the GGA and $\Delta E_B = 1.07$ eV in the LSDA]. Moreover, the distance between the atoms belonging to different dimers is somewhat larger (shorter) when the corresponding local moments are parallel (antiparallel).

The excited isomer closest to the twisted two dimer is a rhomboid with a small isomerization energy ($\Delta E = 0.067$ eV). Here, we also find two separate dimers, that are weakly bounded and have similar characteristics as in the twisted two-dimer structure [see Fig. 4(b)]. It should be noticed that starting the relaxation process with square or rectangular structures it always converge to this rhomboidal geometry. The dimerized linear chain corresponds to a higher energy configuration: as in previous cases, one observes two dimers with a very short bond length and perfectly compensating local magnetic moments (see Table III). The rest of the excited state are a distorted tetrahedron [Fig. 4(d)] with an isomerization energy of $\Delta E = 0.42$ eV followed by two saddle-point structures [Figs. 4(e) and 4(f)].

A similar optimal tetrahedral structure has been found in Ref. 23. In contrast, Kondo *et al.*[21] reported a nondimerized rhombus. Hobbs *et al.*[44] obtained a collinear tetrahedral-like structure with a net zero magnetic moment as ground state. Although a tendency to AF coupling between neighbor atoms was also found in this study, a dimer-based route was not observed.

The obtained LSDA structures and the energy ordering for the lowest isomers is qualitatively similar to the GGA results. Moreover, in the LSDA the twisted two-dimer and rhomboidal geometries are almost degenerated [see Figs. 4(g) and 4(h)]. The most striking difference between LSDA and GGA results is that in the former the first four stationary states are strictly nonmagnetic (i.e., $\mu_i = 0 \ \forall \ i$, in Table III). Although the lack of spin symmetry breaking predicted by the LSDA should be exact for such a finite systems, it probably also reflects a tendency to favor bonding and electron delocalization rather than AF correlations in the local functional. Comparing our results with previous LSDA calculations we observe some qualitative discrepancies. For instance, Cheng and Wang[20] found a dimerized rectangle with AF-coupled local moments as the optimal structure.

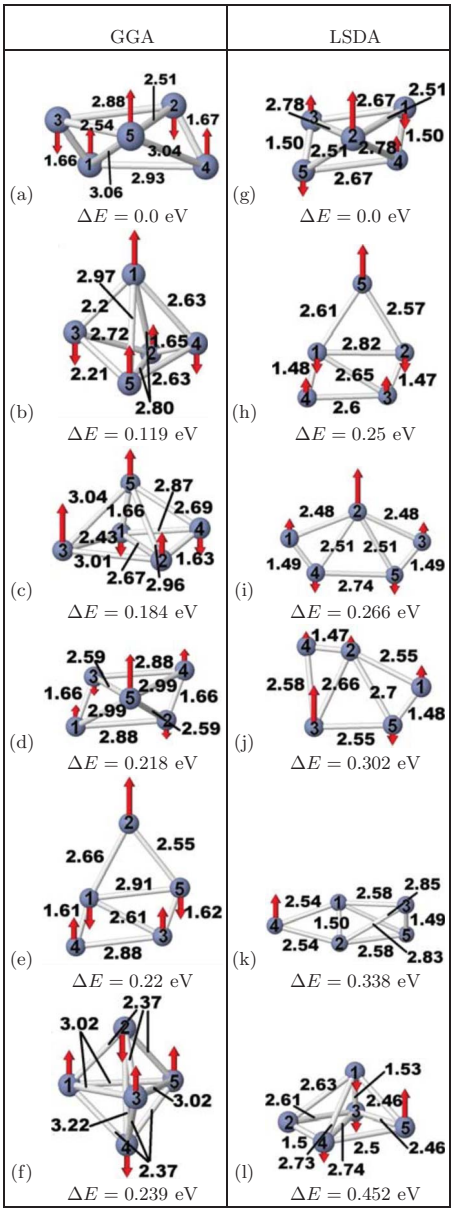

FIG. 5. (Color online) Illustration of the different isomers of Cr_5 found using the GGA and the LSDA. Results are given for the equilibrium bond lengths d_e^{ij} (in Å) and for the energy difference ΔE (in eV) with respect to the optimal structure for each XC functional. The numbers label the different atoms, which local moments are given in Table IV.

TABLE IV. Local magnetic moments μ_i and average moments $\bar{\mu}$ (in μ_B) of the stable isomers of Cr_5 as illustrated in Fig. 5. GGA and LSDA results are compared. The SP are specified.

Isomer	XC	μ_1	μ_2	μ_3	μ_4	μ_5	$\bar{\mu}$
(a)	GGA	2.13	−1.78	−1.93	2.19	4.17	1.2
(g)	LSDA	−0.36	3.98	0.65	0.65	−0.36	1.2
(b)	GGA (SP)	3.79	2.13	−3.19	−1.84	3.79	1.2
(h)	LSDA (SP)	−0.44	−0.49	0.37	0.37	4.12	0.8
(c)	GGA	−1.87	1.91	4.26	−1.84	2.33	1.2
(i)	LSDA	0.1	3.58	0.1	−0.07	−0.07	0.8
(d)	GGA	2.25	−1.97	−1.97	2.25	4.24	1.2
(j)	LSDA	0.67	0.09	4.17	0.15	−0.4	1.2
(e)	GGA	−1.7	4.31	2.01	1.97	−1.8	1.2
(k)	LSDA	−0.07	−0.06	−0.1	4.14	−0.08	0.8
(f)	GGA	3.85	−3.43	3.85	−3.43	3.85	1.2
(l)	LSDA (SP)	−0.28	−0.02	−0.25	−0.23	3.53	0.4

D. Pentamers

The optimized geometries of the low-lying stationary states of Cr_5 obtained with GGA and LSDA functionals are illustrated in Fig. 5. In the case of GGA we also observe a somewhat trend to stabilize structures by forming dimers with intradimer collinear AF coupling and short bond lengths. The lowest-lying geometries are tridimensional and compact indicating that the bonding starts to play a more dominant role in the cluster stability. Indeed, the rhombohedral-base pyramid, which is the most stable structure seems to show the best compromise between increasing coordination and dimer formation. This structure has a rhombohedral base with two dimers in a similar arrangement as in the case of the optimal Cr_4 cluster. The remaining atom ($i=5$) is at the vertex of the pyramid, far away from the base, and has a large atomiclike magnetic moment $\mu_5=4.17\ \mu_B$ [see Fig. 5(a) and Table IV]. This is the reason for the nonvanishing average magnetic moment of $\bar{\mu}=1.2\ \mu_B$, since the local moments of the base atoms sum up to almost zero. Next, it follows a saddle point [a pyramid having a single dimer and magnetic frustrations within the base in Fig. 5(b)] and then, the first excited isomer with similar structure but having two AF bonds (atoms 1 and 3 with $d_{13}=2.43$ Å and atoms 2 and 4 with $d_{24}=1.63$ Å).

The converged planar geometries are low-symmetry structures consisting of two AF-coupled dimers with the fifth atom well separated from the rest at [see, for instance, Fig. 5(e) and Table IV]. This structure has the same average magnetic moment as the ground-state structure but the reduced coordination number makes it less stable. The next stationary state is the trigonal pyramid with no sign of dimerization. All the interatomic distances are comparable to the bulk value (see Fig. 5). An AF-like ordering by layers is observed keeping the same average magnetic moment as the other considered low-energy isomers. Despite being more compact, the absence of dimers renders this structure less stable than the optimal or the first excited isomers. These results are in agreement with the calculations reported by Hobbs *et al.*[44] For the remainder optimized geometries, we also observe a clear trend to dimer formation. However, the reduction in coordination number, particularly in the case of the linear chain, reduces significantly their stability. The values of local and average magnetic moments corresponding to the Cr_5 isomers are summarized in Table IV. It should be noted that our results differ from those reported by Wang *et al.*[23] who obtained dimerization neither for the ground-state structure nor for the first excited isomer. In this work, the first isomer showing dimer growth was very high in energy as compared to the ground state ($\Delta E=1.01$ eV).

Regarding the LSDA optimized geometries, one observes that for a given topology the same trends in the magnetic ordering are obtained as in the case of GGA, but with reduced values of local magnetic moments and bond lengths [see Fig. 5 and Table IV]. This follows the trend observed for smaller cluster sizes as discussed before. Moreover, in contrast to GGA, the LSDA favors planar structures having dimers instead of the more compact geometries [see Figs. 5(h)–5(k)]. Also, notice the different average magnetic moment for different structures in contrast to the results of the GGA functional. Calculations by Cheng and Wang[20] yielded for the optimal geometry a distorted square pyramid with planar base and somewhat large dimer-bond distances.

E. Hexamers

The optimized geometries and values of the average and local magnetic moments obtained with the GGA LSDA functional are illustrated in Fig. 6 and in Table V, respectively.

Concerning to GGA results, we found a distorted trigonal prism as the lowest-energy isomer. This structure possess three dimers at short bond length with AF-like magnetic coupling and zero average magnetic moment. The next stationary states are saddle points [see Figs. 6(b) and 6(c)]. The first one resembles also a trigonal prism but with only two dimers at short bond lengths. The second saddle point presents only one AF dimer at short bond length, and the rest of the dimers with AF-like coupling at a distance comparable to the bulk bond length. The first isomer is illustrated in Fig. 6(d). This

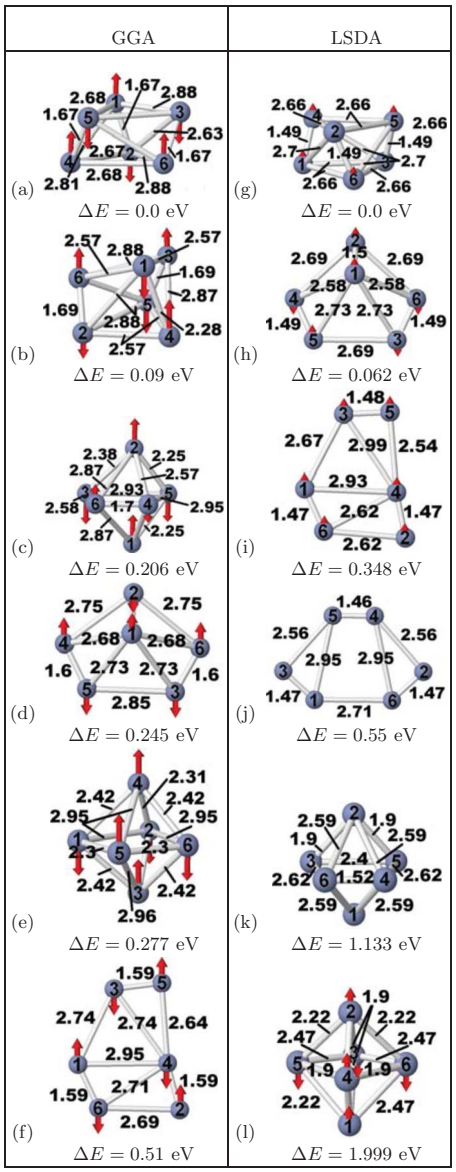

FIG. 6. (Color online) Illustration of the different isomers of Cr_6 found using the GGA and the LSDA. Results are given for the equilibrium bond lengths d_e^{ij} (in Å) and for the energy difference ΔE (in eV) with respect to the optimal structure for each XC functional. The numbers label the different atoms, which local moments are given in Table V.

structure has two AF dimers at short bond lengths and six AF dimers at distance comparable to d_{bulk}. The next most stable structure is the deformed octahedron with an excitation energy of about 0.28 eV, presenting no short bond-length dimers but consisting of several AF-like coupling at bond lengths similar to that of nearest-neighbor bulk distance, probably anticipating the bulklike structure for larger clusters. Finally the less stable structure in Fig. 6 is planar with two dimers at short bond lengths. It should be noticed that here, the number of dimers at bond distances comparable to bulk is five. This is probably the reason that this structure is less stable than that of Fig. 6(d). Moreover, let us remark that the low-coordination structures like the linear chain are at a considerable excitation energy (e.g., 1.84 eV for the linear chain).

For the LSDA functional, the trigonal prism is also found to be the lowest-energy isomer, but the values of the local magnetic moments are notably smaller than the ones found with the GGA functional with a weak FM-like coupling. This is due to the obtained rather short equilibrium bond lengths. Since the average magnetic moment is barely 0.33 μ_B, one can consider this structure to be nearly nonmagnetic. These results are in contrast with those reported by Cheng and Wang,[23] who found a regular trigonal prism as ground state, having AF-like coupling and total magnetic moment of 2 μ_B. The relative order of the next stationary states (isomers and saddle points) changes with respect to the GGA functional, that is to say, the planar structure in Fig. 6(i) becomes now the first excited isomer followed by three saddle-point states in Figs. 6(j)–6(l).

IV. DISCUSSION AND GENERAL TRENDS

The main conclusions on structural and magnetic properties of Cr_N clusters ($N \leq 6$) derived from our calculations can be summarized as follows. (i) The present fully unrestricted noncollinear spin calculations confirm the dimerization trend observed by other authors[20,24] for all $N \leq 6$ and by Wang *et al.*[23] for $N \leq 4$. We always observe that the most stable geometries follow a growth pattern based on dimers with very short bond lengths. The interplay between high coordination and magnetic frustration is always solved by dimerization rather than by noncollinear spin arrangements. (ii) As expected, there is an increasing tendency to favor compact structures over open ones as the cluster size increases. Indeed, already for Cr_4, the binding-energy difference between compact and open geometries is significant. (iii) Concerning the magnetic order one finds that the dimerized structures always correspond to a collinear order with AF-like coupling along short bonds. In some cases, for instance, in the case of the isosceles triangle [see Fig. 3(c)], magnetic frustrations causes the local magnetic moments to be significantly reduced. In other cases, an increase in the distance between atoms showing parallel magnetic moment takes place rather than a reduction in the local moments. Similar parallel alignment of local moments have been observed in small Mn_N clusters.[54] (iv) According to our results, GGA and LSDA approximations considered in this study yield the same general trends in the structural behavior of the Cr clusters. For the considered sizes and for similar structures the magnetic solution given by each functional are different. These differences reflect the way the functionals treat the interplay between hybridization and electronic localization. The most clear example are Cr_2 and Cr_4, where the LSDA approximation gives a nonmagnetic state while the GGA results are magnetic. In the case of Cr_2 we have shown that this is a consequence of the too short LSDA bond length ($d_e^{\text{LSDA}} = 1.47$ Å). Actually, at this distance the hybridization dominates over Coulomb exchange interaction so that the magnetic moments are quenched. However, at the GGA bond length ($d_e^{\text{GGA}} = 1.59$ Å) the LSDA solution becomes magnetic. The trend of overbinding and underestimation of the

TABLE V. Local magnetic moments μ_i and average moments $\bar{\mu}$ (in μ_B) of the stable isomers of Cr_6 as illustrated in Fig. 6. GGA and LSDA results are compared. The SP are specified.

Isomer	XC	μ_1	μ_2	μ_3	μ_4	μ_5	μ_6	$\bar{\mu}$
(a)	GGA	1.97	−1.88	1.82	2.03	−2.03	−1.92	0.0
(g)	LSDA	0.11	0.09	0.09	0.14	0.17	0.17	0.33
(b)	GGA (SP)	−3.68	−2.07	2.06	3.68	−1.96	1.96	0.0
(h)	LSDA(SP)	0.02	0.02	−0.02	−0.02	0.02	−0.02	0.00
(c)	GGA (SP)	3.46	3.46	−3.65	−1.97	−3.4	2.11	0.0
(i)	LSDA	0.02	0.02	−0.02	−0.02	0.027	−0.02	0.0
(d)	GGA	1.89	−1.94	−1.57	1.56	−1.56	1.57	0.0
(j)	LSDA (SP)	0.0	0.0	0.0	0.0	0.0	0.0	0.0
(e)	GGA	−3.44	−3.55	3.44	3.44	3.55	−3.44	0.0
(k)	LSDA (SP)	0.0	0.0	0.0	0.0	0.0	0.0	0.0
(f)	GGA (SP)	1.63	1.72	−1.67	−1.69	1.71	−1.68	0.0
(l)	LSDA (SP)	0.9	0.9	−0.58	0.58	−0.9	−0.9	0.0

bond lengths is a well-known drawback of the LSDA. Due to that reason, the LSDA yields smaller, sometimes vanishing, magnetic moments (see the LSDA results for $N=2$, 4, and 6). The most remarkable case is Cr_4, where all the isomers calculated with the LSDA functional are nonmagnetic. In contrast, the GGA always gives magnetic solutions with significant local magnetic moments. (v) Although throughout this work we attempted to find noncollinear magnetic configurations in all the considered cluster sizes and structures, starting initially from noncollinear magnetic arrangements, they almost always converged to collinear moments. In the case of fixed geometry we found a high-energy state with a noncollinear magnetic arrangement (for instance, the equilateral triangle in Cr_3). Notice, however, that after atomic relaxation, the optimal magnetic solution is always collinear. Despite of the fact that noncollinear magnetism in small freestanding chromium clusters appears to be not stable, it should recalled that it can be stabilized under other conditions. For example, when the clusters are deposited on some magnetic substrates such as Fe or Ni.[55,56]

ACKNOWLEDGMENTS

It is a pleasure to thank J. Rentería and J. C. Sánchez for technical support. This work was supported in part by CONACyT-Mexico through Grants No. 62292 and No. 83642 and by the DAAD-CONACyT exchange program PROALMEX. Computer resources provided by CNS (IPICyT) and the IT Service Center of the University of Kassel are gratefully acknowledged. J.D.D. acknowledges the kind hospitality and support of the University of Kassel, where he spent a sabbatical stay, in the framework of which the final steps of this collaboration have been performed.

[1] J. Bansmann, S. H. Baker, C. Binns, J. A. Blackman, J.-P. Bucher, J. Dorantes-Dávila, V. Dupuis, L. Favre, D. Kechrakos, A. Kleibert, K.-H. Meiwes-Broer, G. M. Pastor, A. Perez, O. Toulemonde, K. N. Trohidou, J. Tuaillon, and Y. Xie, Surf. Sci. Rep. **56**, 189 (2005).

[2] S. Sun, C. B. Murray, D. Weller, L. Folks, and A. Moser, Science **287**, 1989 (2000).

[3] J. T. Lau, A. Föhlisch, R. Nietubyć, M. Reif, and W. Wurth, Phys. Rev. Lett. **89**, 057201 (2002).

[4] N. Fujima, J. Phys. Soc. Jpn. **71**, 1529 (2002).

[5] P. Mavropoulos, S. Lounis, R. Zeller, and S. Blügel, Appl. Phys. A: Mater. Sci. Process. **82**, 103 (2006).

[6] G. M. Pastor, J. Dorantes-Dávila, and K. H. Bennemann, Phys. Rev. B **40**, 7642 (1989).

[7] R. A. Guirado-López, J. Dorantes-Dávila, and G. M. Pastor, Phys. Rev. Lett. **90**, 226402 (2003).

[8] M. B. Knickelbein, Phys. Rev. Lett. **86**, 5255 (2001).

[9] D. Bagayoko, P. Blaha, and J. Callaway, Phys. Rev. B **34**, 3572 (1986).

[10] M. A. Ojeda, J. Dorantes-Dávila, and G. M. Pastor, Phys. Rev. B **60**, 6121 (1999).

[11] S. Lounis, Ph. Mavropoulos, P. H. Dederichs, and S. Blügel, Phys. Rev. B **72**, 224437 (2005).

[12] G. M. Pastor, R. Hirsch, and B. Mühlschlegel, Phys. Rev. Lett. **72**, 3879 (1994).

[13] V. E. Bondybey and J. H. English, Chem. Phys. Lett. **94**, 443 (1983).

[14] S. M. Casey and D. G. Leopold, J. Phys. Chem. **97**, 816 (1993).

[15] F. W. Payne, W. Jiang, and L. A. Bloomfield, Phys. Rev. Lett. **97**, 193401 (2006).

[16] M. M. Goodgame and W. A. Goddard III, Phys. Rev. Lett. **48**, 135 (1982).

[17] B. Delley, A. J. Freeman, and D. E. Ellis, Phys. Rev. Lett. **50**, 488 (1983).

[18] C. W. Bauschlicher, Jr. and H. Partridge, Chem. Phys. Lett. **231**, 277 (1994).

[19] E. J. Thomas III, J. S. Murray, C. J. O'Connor, and P. Politzer, J. Mol. Struct.: THEOCHEM **487**, 177 (1999).
[20] H. Cheng and L.-S. Wang, Phys. Rev. Lett. **77**, 51 (1996).
[21] R. Kondo, R. Sekine, J. Onoe, and H. Nakamatsu, J. Surf. Sci. Soc. Jpn. **21**, 462 (2000).
[22] B. V. Reddy, S. N. Khanna, and P. Jena, Phys. Rev. B **60**, 15597 (1999).
[23] Q. Wang, Q. Sun, B. K. Rao, P. Jena, and Y. Kawasoe, J. Chem. Phys. **119**, 7124 (2003).
[24] J. I. Martínez and J. A. Alonso, Phys. Rev. B **76**, 205409 (2007).
[25] C. Kohl and G. F. Bertsch, Phys. Rev. B **60**, 4205 (1999).
[26] J. E. Peralta, G. E. Scuseria, and M. J. Frisch, Phys. Rev. B **75**, 125119 (2007).
[27] P. Hohenberg and W. Kohn, Phys. Rev. **136**, B864 (1964); W. Kohn and L. J. Sham, *ibid.* **140**, A1133 (1965).
[28] G. Kresse and J. Hafner, Phys. Rev. B **47**, 558 (1993); G. Kresse and J. Furthmüller, *ibid.* **54**, 11169 (1996).
[29] P. E. Blöchl, Phys. Rev. B **50**, 17953 (1994).
[30] G. Kresse and D. Joubert, Phys. Rev. B **59**, 1758 (1999).
[31] Concerning the accuracy of LDA and GGA approximations to DFT in the case of strongly inhomogeneous systems like atoms and small clusters, the reader is referred to the analysis presented in the books quoted in Ref. 32. Despite the expected poor description of the XC hole density $\rho_{\mathrm{XC}}(\vec{r},\vec{r'})$ in the LDA, it is shown there that the local approach gives a good quantitative description of the *spherical average* (SA) of the XC hole density $\rho_{\mathrm{XC}}^{\mathrm{SA}}(\vec{r},s)$ on which the XC energy functional actually depends. This is the result of a systematic cancellation of errors, since $\rho_{\mathrm{XC}}^{\mathrm{LDA}}$ satisfies the exact sum rule $\int \rho_{\mathrm{XC}}^{\mathrm{LDA}}(\vec{r},\vec{r'})d^3r' = -1$.
[32] R. G. Parr and W. Yang, *Density-Functional Theory of Atoms and Molecules* (Oxford University Press, New York, 1989), pp. 186–194; R. M. Dreizler and E. K. U. Gross, *Density Functional Theory* (Springer-Verlag, Berlin, 1990), pp. 186–187.
[33] D. M. Ceperley and B. J. Alder, Phys. Rev. Lett. **45**, 566 (1980).
[34] S. H. Vosko, L. Wilk, and M. Nusair, Can. J. Phys. **58**, 1200 (1980).
[35] J. P. Perdew, K. Burke, and M. Ernzerhof, Phys. Rev. Lett. **77**, 3865 (1996).
[36] N. D. Mermin, Phys. Rev. **137**, A1441 (1965); A. De Vita, Ph.D. thesis, Keele University, 1992; A. De Vita and M. J. Gillan, J. Phys.: Condens. Matter **3**, 6225 (1991).
[37] U. von Barth and L. Hedin, J. Phys. C **5**, 1629 (1972); J. Kübler, K.-H. Höck, J. Sticht, and A. R. Williams, J. Appl. Phys. **63**, 3482 (1988); J. Phys. F: Met. Phys. **18**, 469 (1988).
[38] N. A. Baykara, B. N. Mcmaster, and D. R. Salahub, Mol. Phys. **52**, 891 (1984).
[39] P. Ruiz-Díaz, J. Dorantes-Dávila, and G. M. Pastor, Eur. Phys. J. D **52**, 175 (2009).
[40] P. Ruiz-Díaz, R. Garibay-Alonso, J. Dorantes-Dávila, and G. M. Pastor (unpublished).
[41] G. Rollmann, P. Entel, and S. Sahoo, Comput. Mater. Sci. **35**, 275 (2006).
[42] T. Oda, A. Pasquarello, and R. Car, Phys. Rev. Lett. **80**, 3622 (1998).
[43] G. Henkelman, A. Arnaldsson, and H. Jónsson, Comput. Mater. Sci. **36**, 354 (2006); E. Sanville, S. D. Kenny, R. Smith, and G. Henkelman, J. Comput. Chem. **28**, 899 (2007); W. Tang, E. Sanville, and G. Henkelman, J. Phys.: Condens. Matter **21**, 084204 (2009).
[44] D. Hobbs, G. Kresse, and J. Hafner, Phys. Rev. B **62**, 11556 (2000).
[45] D. L. Michalopoulos, M. E. Geusic, S. G. Hansen, D. E. Powers, and R. E. Smalley, J. Phys. Chem. **86**, 3914 (1982).
[46] K. Hilpert and K. Ruthardt, Ber. Bunsenges. Phys. Chem. **91**, 724 (1987).
[47] E. A. Rohlfing and J. J. Valentini, J. Chem. Phys. **84**, 6560 (1986).
[48] J. Harris and R. O. Jones, J. Chem. Phys. **70**, 830 (1979).
[49] K. Andersson, B. O. Roos, P. A. Malmqvist, and P. O. Widmark, Chem. Phys. Lett. **230**, 391 (1994).
[50] B. O. Roos and K. Andersson, Chem. Phys. Lett. **245**, 215 (1995).
[51] N. E. Schultz, Y. Zhao, and D. G. Truhlar, J. Phys. Chem. A **109**, 4388 (2005).
[52] R. Hafner, D. Spisák, R. Lorenz, and J. Hafner, J. Phys.: Condens. Matter **13**, L239 (2001); **14**, 2119 (2002) (erratum); S. Cottenier, B. de Vries, J. Meersschaut, and M. Rots, *ibid.* **14**, 3275 (2002); R. Hafner, D. Spisák, R. Lorenz, and J. Hafner, Phys. Rev. B **65**, 184432 (2002).
[53] S. Lounis, P. Mavropoulos, R. Zeller, P. H. Dederichs, and S. Blügel, Phys. Rev. B **75**, 174436 (2007).
[54] J. Mejía-López, A. H. Romero, M. E. Garcia, and J. L. Morán-López, Phys. Rev. B **74**, 140405(R) (2006).
[55] R. Robles and L. Nordström, Phys. Rev. B **74**, 094403 (2006).
[56] S. Lounis, M. Reif, P. Mavropoulos, L. Glaser, P. H. Dederichs, M. Martins, S. Blügel, and W. Wurth, EPL **81**, 47004 (2008).